Volume 1 | Number 1 | Jan 2013 | Pages 1–100

Journal of
**Materials Chemistry B**

Materials for biology and medicine
www.rsc.org/materialsB

ROYAL SOCIETY
OF CHEMISTRY

ROYAL SOCIETY
OF CHEMISTRY

www.rsc.org/materialsB

**Facilitated biosensing *via* direct electron transfer of myoglobin integrated into diblock copolymer/multi-walled carbon nanotube nanocomposites**

Victoria V. Shumyantseva[1], Larisa V. Sigolaeva[2*], Liubov E. Agafonova[1], Tatiana V. Bulko[1], Dmitry V. Pergushov[2], Felix H. Schacher[3,4], Alexander I. Archakov[1]

[1] *Institute of Biomedical Chemistry, Pogodinskaya St. 10, Moscow 119121, Russia*

[2] *Department of Chemistry, Lomonosov Moscow State University, 119991 Moscow, Russia*

[3] *Institute of Organic and Macromolecular Chemistry, Friedrich-Schiller-University Jena, D-07743 Jena, Germany*

[4] *Jena Center for Soft Matter (JCSM), Friedrich-Schiller-University Jena, D-07743 Jena, Germany*

*corresponding author:

Larisa V. Sigolaeva, lsigolaeva@genebee.msu.ru

**Abstract**

Nanocomposite materials were prepared by sequential drop casting of multi-walled carbon nanotube (MWCNT) suspensions and amphiphilic polybutadiene-*block*-poly(2-(*N,N*-dimethylamino)ethyl methacrylate) (PB$_{290}$-*b*-PDMAEMA$_{240}$) diblock copolymer micelles on screen-printed electrodes (SPEs). This nanocomposite material was found to be very favorable for integration of myoglobin (Mb) and facilitates a direct electron transfer from an electrode to

1

heme proteins. In that respect, $PB_{290}$-*b*-$PDMAEMA_{240}$ was demonstrated to be a well-suited binding agent. In aqueous solutions, the diblock copolymer forms core-corona micelles (shown by cryogenic transmission electron microscopy, cryo-TEM, and nanoparticle tracking analysis, NTA), which at pH 7 in phosphate buffer exhibit good adhesion to carbon materials (shown by atomic force microscopy, AFM, scanning electron microscopy, SEM, and scanning transmission electron microscopy, STEM) and builds up uniform thin films on a hydrophobic graphite-based substrate. As demonstrated by a quartz crystal microbalance with dissipation monitoring (QCM-D), attractive interactions of Mb and $PB_{290}$-*b*-$PDMAEMA_{240}$ take place when both components are subsequently deposited onto a solid substrate. Spectroscopic studies confirmed that the absorption maximum of Mb remains unaltered, suggesting that at least some protein globules retain their tertiary structure. Cyclic voltammetry and square wave voltammetry show a remarkable (ca 180-fold) increase of the reductive current of Mb after its incorporation into the $SPE/MWCNTs/PB_{290}$-*b*-$PDMAEMA_{240}$ matrix. The herein developed analytical approach was used for the detection of cardiac myoglobin as a very early marker of acute myocardial infarction (AMI) both in plasma of healthy donors and patients with AMI.

## Introduction

Hemeproteins play an important role in biochemical events such as transport and storage of molecular oxygen by hemoglobin (Hb) and myoglobin (Mb), the transfer of electrons from respiratory substrates by cytochromes and the terminal oxidation with $O_2$ by cytochrome c oxidase, the decomposition of hydrogen peroxide by catalase, the oxidation of organic substances with $H_2O_2$ by peroxidase, the metabolic conversion of drugs and xenobiotics by Phase I enzymes cytochromes P450, the synthesis of nitric oxide from l-Arg by NO synthase, and the utilization of reactive oxygen species with catalase. As a matter of fact, all these different functions are primarily based upon the oxidation/reduction properties of the heme iron itself according to the scheme $Fe(III) + e^- + H^+ \rightleftarrows Fe(II)$.[1, 2]

Quantitative detection of the heme protein Mb at low concentrations in human biological fluids is still challenging. Acute Myocardial Infarction (AMI) affects millions of people each year, many of whom die because diagnosis or treatment was not available in time. Indeed, cardiovascular disease is the reason of nearly half of all deaths in the Western world[3] and over half of all deaths in Russia.[4] Studies have shown that if a correct diagnosis of AMI, and appropriate therapeutic intervention is performed within the first 6 hours after the onset of chest pain, the chances of survival are greatly increased. In AMI patients, blood, serum, and plasma cardiac myoglobin (c-Mb) levels are known to be up to 10-fold above normal as early as 30 minutes after the onset of chest pain.[5] Thus, monitoring the rapid release of c-Mb can be used as a very early biomarker of AMI.[6] From this viewpoint, biomedical devices and point-of-care sensors for c-Mb detection are in-demand.

Biosensing of Mb operates through direct electron transfer reactions (with electrons being directly transmitted between the electrode and the heme iron of Mb) and belong to the third-generation of biosensors.[7] Efficiency of direct electron transfer between the electrode and the heme depends on the employed electrode material, electrode surface modification and proper orientation of the active protein center on the electrode. Plural breakthroughs in registration of

direct electron transfer and in third-generation biosensors are addressed to the development of various types of modification of working (indicator) electrodes and, especially, to the creation of composite nanomaterials. Composite nanomaterials are expected to improve electronic transport, promote anchoring biological material on an electrode surface, and impart biocompatibility for the preservation of native, affine, and catalytic properties of biomolecules.

Various materials are used as components of nanocomposites including natural and synthetic polymers,[8-15] synthetic surfactants such as didodecyldimethylammonium bromide (DDAB),[16, 17] metal or metal oxide nanoparticles,[18] and nanomaterials with various spatial organizations,[19, 20] in particular based on carbon – graphene, graphene oxide, single-walled carbon nanotubes (SWCNTs), and multi-walled carbon nanotubes (MWCNTs).[21-25] Carbon nanotubes are among the most commonly applied in bioelectrochemistry due to their electrochemically inert surface and good thermal and electrochemical stability. Although data regarding the biocompatibility of carbon nanotubes is inconsistent,[26] nanostructuring of electrode surfaces by carbon nanotubes increases the sensitivity for the detection of electron transfer processes.[22, 23, 27]

The compatibility between different components in nanocomposites is of distinctive importance for the final properties of the material. In case of organic/inorganic combinations, amphiphilic block copolymers containing both a non-polar and a polar, chargeable block would be desirable, although literature examples are still relatively rare.[28] Specifically, amphiphilic diblock copolymers based on polybutadiene (PB) and poly(2-(*N,N*-dimethylamino)ethyl methacrylate) (PDMAEMA) [29] seem to be promising as interlink between carbon nanomaterials and biomolecules. Indeed, the presence of hydrophobic low glass transition temperature, $T_g$, domains might facilitate the modification of hydrophobic carbon surfaces while the hydrophilic, chargeable segments can bind biomaterials.

The adsorption of diblock copolymer micelles onto planar surfaces has been intensively studied[30-32] for various substrates[33] as well as varying adsorption conditions.[34, 35] However, such

approaches are still new in the context of biosensor applications.[36-39] We have recently described the use of amphiphilic diblock copolymer micelles for the adsorption of enzymes onto graphite substrates to construct biosensors for phenol and choline, respectively.[38, 39] Based on surface imaging techniques, we could demonstrate that the most effective surface coverage of graphite is achieved if the adsorption is carried out in the presence of strong screening counterions for strong polyelectrolytes (charge-suppressed state)[40] or at the respective pH value in case of weak polyelectrolytes.[38, 39] This led to the subsequent deposition of an increased amount of enzyme and, therefore, to higher enzymatic activity of the entire construct.

In the present work, we report the fabrication of nanocomposite materials based on MWCNTs and an amphiphilic $PB_{290}$-$b$-$PDMAEMA_{240}$ diblock copolymer via drop casting on a surface of SPE, where $PB_{290}$-$b$-$PDMAEMA_{240}$ acts both as compatibilizer and binding agent (the subscripts denote the number-average degree of polymerization of the corresponding block). This nanocomposite was found to be well-suited for facilitation of direct electron transfer of integrated Mb from an electrode to a heme protein. Thus, these materials can be used as sensitive and smart biosensors for Mb detection.

**Experimental Part**

**Materials.** Myoglobin (from equine skeletal muscle) was purchased from Sigma. Multi-walled carbon nanotubes (MWCNTs) with the outer diameter of 10-15 nm, the inner diameter of 2-6 nm, and lengths of 0.1-10 μm were obtained from Sigma-Aldrich. Mouse anti-human myoglobin, cardiac M9800-16A (Ab$^{Mb}$, supplied as 1.05 mg/ml solution in phosphate buffer saline of pH 7.4 with 0.1 % sodium azide) was obtained from USBiological. Phosphate buffer solutions with NaCl (100 mM potassium phosphate with 50 mM NaCl) at specified pHs were prepared by mixing stock solutions of 100 mM $KH_2PO_4$ and 100 mM $K_2HPO_4$ (both containing 50 mM NaCl) to the desired pH value. All other chemicals were of analytical grade and used without further purification. All aqueous solutions were prepared using Milli-Q water (18.2 MΩcm) purified with a Milli-Q water purification system by Millipore.

Plasma samples were obtained from healthy donors (HDs) and patients with acute myocardial infarction (AMI). Informed signed consent was received from each of the patients. Plasma of HDs and patients with AMI was collected after centrifugation of blood with EDTA as anticoagulant for 10 min at 3000 rpm. Myoglobin concentration in plasma samples was determined with the bench-top lateral flow RAMP® (Response Biomedical Corp) immunoassay as described in.[41, 42]

**Synthesis of PB$_{290}$-*b*-PDMAEMA$_{240}$.**[43] The synthesis of PB$_{290}$-*b*-PDMAEMA$_{240}$ was accomplished in THF by sequential anionic polymerization using *sec*-BuLi as initiator. At -70 °C, *sec*-BuLi was added to THF followed by fast addition of butadiene. The conversion was monitored *via* a NIR probe. After a reaction time of 10 h at -10 °C, 2 equiv. 1,1-diphenylethylene were added *via* syringe to endcap the living chain ends. After 1 h, *N*,*N*-(dimethylamino)ethylmethacrylate (DMAEMA) was added to the reaction mixture *via* syringe and stirred for 2 h at -50 °C. The diblock copolymer was purified by precipitation in water.

**Nanoparticle tracking analysis (NTA).** The sample of diblock copolymer micelles was diluted to a concentration suitable for the analysis with Milli-Q water, which was primarily filtered 3

times through Nylon filters (Millipore) with a pore size of 0.2 μm. All measurements were performed on a Nanosight LM10 configuration HSBF with a 405 nm diode laser (65 mW) and EMCCD Andor Lucc high-sensitivity camera (Salisbury, UK) according to the ASTM E 2834-12 protocol. The experiment was started with an initial test of filtered Milli-Q water to ensure no nanoparticle contamination, after which the diluted sample of micelles was injected into the sample chamber and was measured for 60 s with manual shutter and gain adjustments. The measurements were repeated until the number of tracks analyzed reaches to at least 2000. After capture, the particle size distribution was determined using the NTA software NTA 2.3 Build 0033.

**Potentiometric titration.** Potentiometric titration of $PB_{290}$-*b*-$PDMAEMA_{240}$ was performed using a digital pH meter (Orion) equipped with a combined glass/reference electrode, calibrated with standard buffer solutions of pH 4.0, 7.0, and 10.0 (Oacton, Orion). The titration of $PB_{290}$-*b*-$PDMAEMA_{240}$ was started from the initial pH value of an aqueous solution with the concentration of 0.005 M in terms of DMAEMA units. 10 mM HCl was used as the titrant, which was added by 10 μl portions to a 1.5 ml sample of diblock copolymer solution at a constant temperature (25 °C) and under intensive stirring. pH readings were registered after establishing the equilibrium state when the pH reached a constant value after each step of titrant addition. The degree of protonation α of the PDMAEMA block was calculated as the molar ratio of the added titrant to the DMAEMA units of $PB_{290}$-*b*-$PDMAEMA_{240}$. For the calculation of the $pK_a$ values, the Henderson-Hasselbalch equation was used.

**Quartz crystal microbalance with dissipation monitoring (QCM-D).** The adsorption of $PB_{290}$-*b*-$PDMAEMA_{240}$ micelles and Mb was followed *in-situ* by QCM-D (Q-Sense, E1 system). The sensor crystals (Q-Sense) were AT-cut quartz with gold-plated polished electrodes. The quartz crystals were excited at their fundamental frequency ($f_0 \approx 5$ MHz) as well as at the 3rd, 5th, 7th, 9th, and 11th overtones, corresponding to 15, 25, 35, 45, and 55 MHz, respectively. Before use, the crystals were cleaned according to the Q-Sense cleaning protocol by sequential

ozone treatment for 10 min, then treatment by a mixture of Milli-Q/NH$_4$OH/H$_2$O$_2$ = 5:1:1 at 70

°C for 10 min, followed by rinsing with Milli-Q water, blowing by air flux, and again ozone

treatment for 10 min. Before the experiment was started, the resonance frequency and dissipation

found for each overtone were set equal to zero. Each QCM-D experiment was started from

baseline recording for the 100 mM potassium phosphate with 50 mM NaCl of pH 8.2. Then, the

PB$_{290}$-$b$-PDMAEMA$_{240}$ micelles were first adsorbed from the solutions in the same buffer,

followed by a washing step with the initial buffer to remove any loosely attached material. For

protein adsorption studies, Mb (100 µM in 100 mM potassium phosphate with 50 mM NaCl of

pH 7.4) was deposited on the pre-adsorbed PB$_{290}$-$b$-PDMAEMA$_{240}$ layer in the same way.

Thereafter, a protein-free 100 mM potassium phosphate with 50 mM NaCl of pH 7.4 was used to

remove weakly adsorbed protein molecules. During each adsorption stage, frequency and

dissipation shifts were continuously recorded as a function of time. For all experiments, the

temperature was set to 25 °C.

**Atomic force microscopy (AFM).** For AFM imaging of the formed PB$_{290}$-$b$-PDMAEMA$_{240}$

films, freshly cleaved HOPG was used (as slices of about 5mm×10mm). PB$_{290}$-$b$-PDMAEMA$_{240}$

micelles were adsorbed onto HOPG at ambient temperature by covering the HOPG slide with a

drop of a 1 mg/ml solution of PB$_{290}$-$b$-PDMAEMA$_{240}$ in 50 mM potassium phosphate of pH 7,

followed by 1 hour adsorption. After that time, the substrate was rinsed with Milli-Q water and

shortly blown by a stream of air. Prior to any AFM measurements, the samples were kept in a

desiccator with silica gel for at least 30 min. AFM images were taken with a commercial atomic

force microscope (DI Dimension 3100 Metrology™) operating in TappingMode™ and using

Si$_3$N$_4$ cantilevers (OMCLAC160TS, Olympus) with a typical spring constant of 42 N/m, a

typical resonance frequency of 300 kHz, and a tip radius of less than 7 nm. For imaging, light

tapping (ratio of set point amplitude to free amplitude ~0.9) was applied. Each AFM result was

presented as typical image chosen on the basis of at least three uniform-sized images obtained

from different places of each AFM sample. Images were analyzed using the NanoScope Analysis software version 1.20.

**Cryogenic Transmission Electron Microscopy (cryo-TEM).** For cryo-TEM studies, a drop (~2 μL) of the sample solution (c = 0.25 wt %) was placed on a plasma-treated lacey carbon-coated copper TEM grid (200 mesh, Science Services, Münich, Germany), then most of the liquid was removed with blotting paper, leaving a thin film stretched over the grid holes. The specimens were instantly vitrified by rapid immersion into liquid ethane in a temperature-controlled freezing unit (Zeiss Cryobox, Zeiss NTS GmbH, Oberkochen, Germany) and cooled to approximately 90 K. The temperature was monitored and kept constant in the chamber during all preparation steps. After freezing the specimens, they were inserted into a cryo-transfer holder (CT3500, Gatan, Münich, Germany) and transferred to a Zeiss EM922 Omega instrument (Carl Zeiss Microscopy GmbH, Oberkochen, Germany). Examinations were carried out at temperatures around 90 K. The transmission electron microscope was operated at an acceleration voltage of 200 kV. Zero-loss filtered images ($\Delta E$ = 0 eV) were taken under reduced dose conditions. All images were registered digitally by a bottom-mounted CCD camera system (Ultrascan 1000, Gatan, Münich, Germany), combined, and processed with a digital imaging processing system (Gatan Digital Micrograph 1.82) and UTHSCSA Image Tool 3.00.

**Electron Microscopy.** The STEM/SEM images were obtained by S-5500 Hitachi Electron Microscope operated at 25 kV. Samples for STEM/SEM analysis were taken for the same 400 mesh carbon-coated copper grid consequently modified by drop casting of 2 μl of specified solution, allowing the solvent to evaporate and shortly washing with Milli-Q water to remove salts. The tested solutions were: MWCNTs suspension in chloroform, 0.5 mg/ml solution of $PB_{290}$-$b$-$PDMAEMA_{240}$ in 100 mM potassium phosphate with 50 mM NaCl of pH 8.2, and 100 μM of sk-Mb in 100 mM potassium phosphate with 50 mM NaCl of pH 7.4.

**Preparation of electrochemical sensors.** Three-pronged screen-printed electrodes (SPEs) purchased from AVTOKOM (Russia, Moscow, http://www.avtocom-moscow.ru) were used for

the electrodes preparation. They consist of a round graphite working electrode of 2 mm in diameter surrounded with a graphite ringed auxiliary counter-electrode and an Ag/AgCl pseudo-reference electrode. For $PB_{290}$-*b*-$PDMAEMA_{240}$/Mb film assembly, 2 µL of $PB_{290}$-*b*-$PDMAEMA_{240}$ (0.5 mg/ml or 2 mg/ml in 100 mM potassium phosphate with 50 mM NaCl of pH 8.2) were dropped onto 2 mm area of the working electrode and incubated for 15 min until complete drying. Then, 2 µL of 100 µM of Mb in 100 mM potassium phosphate with 50 mM NaCl of pH 7.4 were applied. The electrodes were then kept at +4 °C overnight. For $MWCNTs/PB_{290}$-*b*-$PDMAEMA_{240}$/Mb film assembly, 1 mg of MWCNTs was suspended in 1 ml of chloroform by sonication of the mixture for 1 min at 38 W. The electrodes were first modified with 2 µL of freshly prepared MWCNTs suspension. After chloroform evaporation for 10 min, the films of $PB_{290}$-*b*-$PDMAEMA_{240}$ and Mb were formed as described above. For preparation of electrochemical immunosensors, antibodies to myoglobin ($Ab^{Mb}$) were immobilized onto the $MWCNTs/PB_{290}$-*b*-$PDMAEMA_{240}$ (2mg/ml) electrode by drop casting of 1 µl of 105 ng/µl $Ab^{Mb}$ solution in 100 mM potassium phosphate with 50 mM NaCl of pH 7.4. The electrodes were then kept at +4 °C overnight.

**Electrochemical measurements.** Cyclic voltammetry (CV) and square wave voltammetry (SWV) measurements were performed using an Autolab electrochemical system (Eco Chemie, Utrecht, The Netherlands) equipped with PGSTAT-12 and GPES software (Eco Chemie, Utrecht, The Netherlands). All electrochemical experiments were carried out at room temperature in 100 mM potassium phosphate with 50 mM NaCl of pH 7.4. CV experiments were carried out in a 1 mL electrochemical cell from an initial potential of –0.7 V to the end-point potential of +0.4 V at different scan rates. Alternatively, SWV experiments were carried out in a 100 µL drop applied onto the SPE so as to cover all 3 electrodes at the following experimental SWV parameters: the initial potential of 0.1 V, the end potential of –0.6 V, the amplitude of 20 mV, the step height of 5 mV; the frequency of 10 Hz. All potentials were referred to the Ag/AgCl screen-printed pseudo-reference electrode. For the electrochemical analysis of human

blood plasma samples, 1 µL of undiluted plasma taken from a HD or the AMI patient was placed onto the SPE/MWCNTs/PB$_{290}$-*b*-PDMAEMA$_{240}$/Ab$^{Mb}$ immunosensor surface and allowed to stay for 15 min at 37 °C. To reduce unspecific binding, the immunosensors were placed in the cell with 100 mM potassium phosphate with 50 mM NaCl of pH 7.4 for 15 min at room temperature. The CV voltammograms were recorded from −0.7 V to +0.4 V at 50 mV/s.

**Spectral assay.** Spectral studies were performed using a Cary 100 Scan UV-Vis spectrophotometer with the Cary WinUV software (Agilent, USA). Absorption spectra of sk-Mb were recorded after application of 6 µL of the PB$_{290}$-*b*-PDMAEMA$_{240}$ solution and then 6 µL of 100 µM Mb onto transparent polyvinylchloride plates (4 mm×2.5 mm). After drying and washing with 100 mM potassium phosphate with 50 mM NaCl of pH 7.4 plates were placed in standard 1.5 mL spectral polystyrene cuvettes for spectrum recording. Plates covered with PB$_{290}$-*b*-PDMAEMA$_{240}$ were used as a negative control and 25 µM solutions of sk-Mb in 100 mM potassium phosphate with 50 mM NaCl of pH 7.4 was used as positive control.

**Results and discussion**

**1. PB$_{290}$-$b$-PDMAEMA$_{240}$ solution properties**

In this study, we used an amphiphilic diblock copolymer, polybutadiene-*block*-poly(2-(*N,N*-dimethylamino)ethyl methacrylate) (PB$_{290}$-$b$-PDMAEMA$_{240}$), where the subscripts denote the number-average degrees of polymerization of the corresponding blocks, with a molecular weight of 53500 g/mol (PDI = 1.1). The chemical structure of the diblock copolymer is shown in Fig. 1A. PB$_{290}$-$b$-PDMAEMA$_{240}$ comprises both a hydrophobic PB (with a low glass transition temperature, T$_g$, of -15 °C) and a hydrophilic PDMAEMA block (depending on the solution pH and the temperature).[44]

First, the self-assembly of PB$_{290}$-$b$-PDMAEMA$_{240}$ in aqueous media was examined. Nanoparticle tracking analysis (NTA) shows the presence of particles with an average diameter of 106 nm (averaged value was obtained based on the analysis of about 6000 tracks, Fig. 1B). The obtained results clearly indicate the formation of aggregates (micelles) in aqueous solutions of PB$_{290}$-$b$-PDMAEMA$_{240}$.

The core–corona structure of the aggregates featuring a hydrophobic PB core and a cationic corona built up from PDMAEMA was visualized by cryogenic transmission electron microscopy (cryo-TEM). Fig. 1C shows a cryo-TEM micrograph of PB$_{290}$-$b$-PDMAEMA$_{240}$ micelles at pH 7 as objects with spherical shape and a moderately broad size distribution. A darker hydrophobic PB core with a mean diameter of 38±8 nm (averaged value was obtained from approximately 115 micelles) is visible in the center of the objects. The water-soluble PDMAEMA corona is only partially visible (in the vicinity of the PB core) in the cryo-TEM micrograph due to its lower electron contrast. Its thickness can be roughly evaluated as > 34 nm from both NTA and cryo-TEM data though the higher ionic strength (50 mM sodium phosphate) in the cryo-TEM samples might lead to larger core size due to salt-induced increase of the aggregation number as has been shown for dynamic micelles.[45] These determinations of the size of the PB core and the overall size of the micelles found for PB$_{290}$-$b$-PDMAEMA$_{240}$ are in good

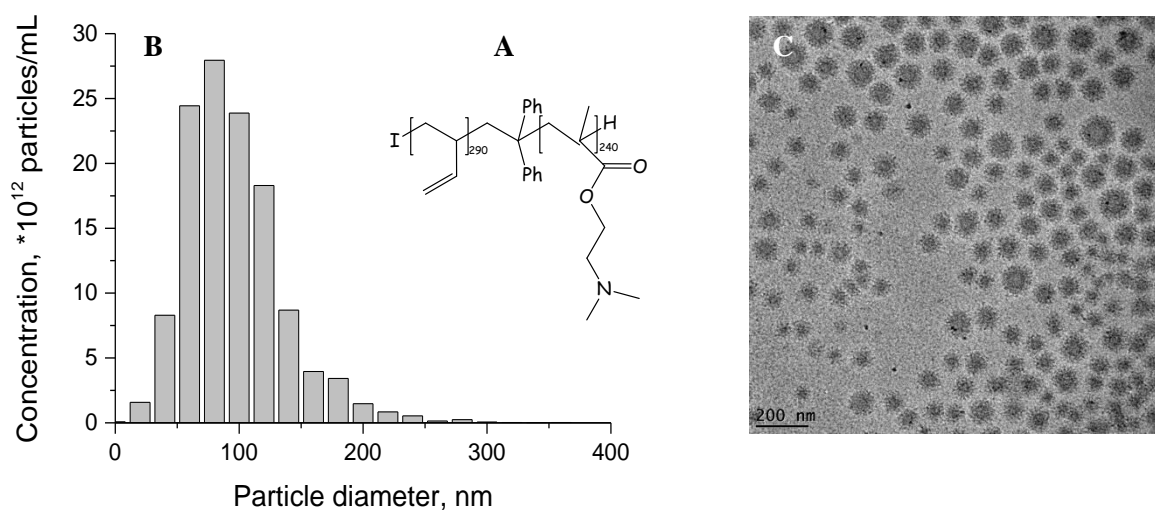agreement with former data reported for diblock copolymers of similar structure and composition.[38, 39]



Fig. 1. Chemical structure of $PB_{290}$-$b$-$PDMAEMA_{240}$ (A), NTA plot for $PB_{290}$-$b$-$PDMAEMA_{240}$ micelles in aqueous solution (c = $5.0 \times 10^{-5}$ mg/ml) (B), and cryo-TEM micrograph of $PB_{290}$-$b$-$PDMAEMA_{240}$ micelles (C) in 50 mM sodium phosphate (c $\approx$ 2.5 mg/ml) at pH 7.0.

As PDMAEMA is a weak polyelectrolyte, the charge and the solution structure (e.g., corona extension) of these micelles are pH-dependent. To understand the effect of the pH, the charge of $PB_{290}$-$b$-$PDMAEMA_{240}$ was investigated by potentiometric titration (Fig. 2). Titration with 10 mM HCl results in complete protonation of the ternary amino group (Fig. 2B). Assuming $\alpha$ as the protonation degree of the PDMAEMA block (see also the description given in Fig. 2) and determining $\alpha=0$ at the initial pH of the $PB_{290}$-$b$-$PDMAEMA_{240}$ solution and $\alpha=1$ at the point of inflection of the curve [pH $vs.$ V of titrant added], one can plot the dependence of the protonation degree $\alpha$ of the PDMAEMA block on the pH [$\alpha$ $vs.$ pH] (Fig. 2A). According to this dependence, PDMAEMA undergoes a conversion from the fully protonated (charged) state to the fully deprotonated (non-charged) state in the pH range of 4.0-8.5. Although these values refer to the solution state of the PDMAEMA block, we assume that they can be extended to the adsorbed state of $PB_{290}$-$b$-$PDMAEMA_{240}$ as well.

The data on the $pK_a^{char.}$ ($\alpha=0$) and $pK_a^{app.}$ ($\alpha=0.5$) for $PB_{290}$-$b$-$PDMAEMA_{240}$ determined according to the Henderson-Hasselbalch equation were found to be 6.7 and 6.35, respectively

(Fig. 2C). The value of $pK_a$s were found to be in good agreement with $pK_a$s found for diblock copolymers with similar structure,[38] for $pK_a^{app.}$ ($\alpha$=0.5) of star-shaped PDMAEMAs,[46] and comparable with the values of $pK_a^{app.}$ ($\alpha$=0.5) found for other linear and star-shaped PDMAEMAs.[44, 47]
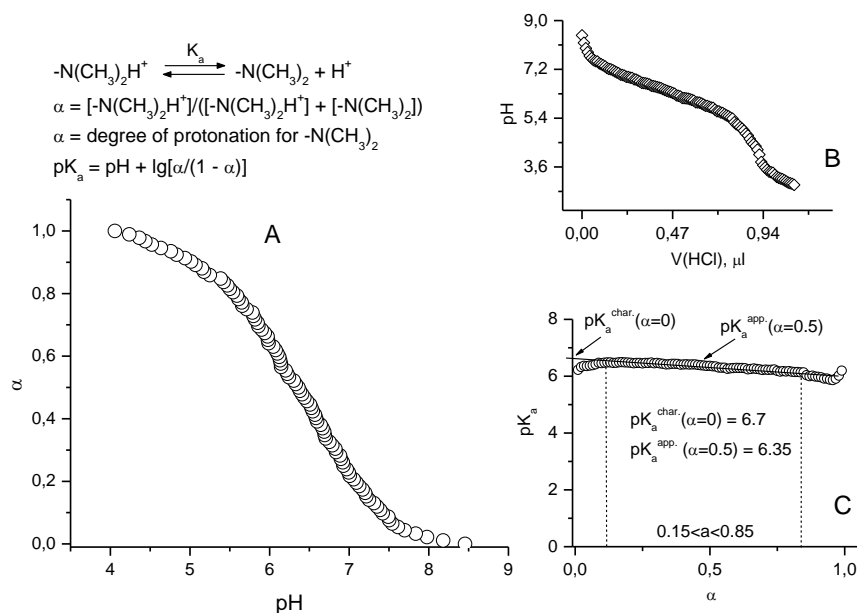


Fig. 2. Dependence of the protonation degree $\alpha$ of the PDMAEMA block on the pH in water (A). the initial potentiometric titration curve of $PB_{290}$-$b$-$PDMAEMA_{240}$ (B); and the dependence of $pK_a$ on the protonation degree $\alpha$ for $PB_{290}$-$b$-$PDMAEMA_{240}$ block determined according to the Henderson-Hasselbalch equation (C). The diblock copolymer concentration was 5 mM (in terms of the concentration of DMAEMA units). The titration was started from pH 8.48 and was performed by stepwise addition of 10 $\mu$L of 10 mM HCl.

This pH-dependence of the charge of $PB_{290}$-$b$-$PDMAEMA_{240}$ allows us to predict the interaction of its micelles with a hydrophobic solid surface. Deprotonation of the PDMAEMA segments together with effective PDMAEMA charge screening induced by the presence of phosphate and chloride counterions (from 100 mM potassium phosphate with 50 mM NaCl) will obviously shift PDMAEMA into the non-charged state and should facilitate the drift of such micelles from the water phase to the hydrophobic solid support, followed by adsorption.

**2. Solid interface interactions and characterization of the films**

The films formed by $PB_{290}$-*b*-$PDMAEMA_{240}$ on a surface of highly oriented pyrolytic graphite (HOPG) were characterized by atomic force microscopy (AFM) in the dry state. HOPG was used as model system to study the adsorption characteristics. The surface of freshly cleaved HOPG is very smooth within a single terrace ($R_a$ < 1 nm) and relatively hydrophobic with an air contact angle value of 85.1±4.3.[39] It was found that $PB_{290}$-*b*-$PDMAEMA_{240}$ micelles at pH 7.0 are adsorbed on HOPG, forming films with high surface coverage although with hollowed structure probably due to some dewetting (Fig. 3). The mean thickness of $PB_{290}$-*b*-$PDMAEMA_{240}$ film was about 2 nm. Despite the fact that cryo-TEM clearly revealed the presence of spherical micelles in aqueous solution of $PB_{290}$-*b*-$PDMAEMA_{240}$, no single self-assembled aggregates are visible after their direct adsorption onto the substrate. It suggests that the interaction of $PB_{290}$-*b*-$PDMAEMA_{240}$ micelles with HOPG disturbs their dynamic (low $T_g$ of PB) micellar structure and induces strong interactions of the hydrophobic (PB) block with the substrate, leading to the disruption of the spherical self-assemblies.
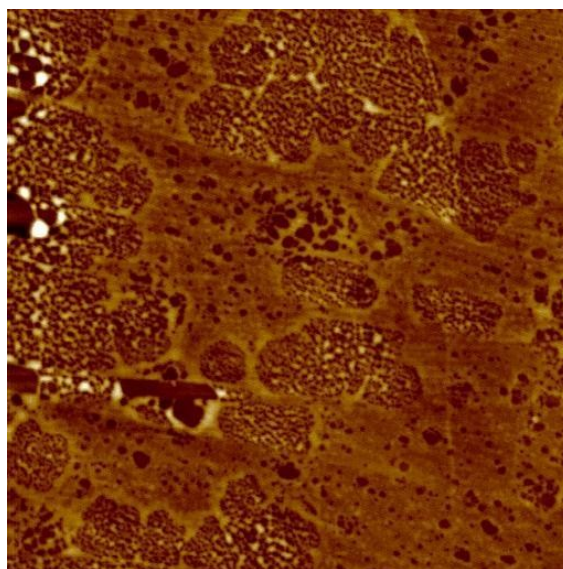


Fig. 3. Typical 3×3 μm AFM height image taken in the dry state of a $PB_{290}$-*b*-$PDMAEMA_{240}$ film adsorbed on HOPG at pH 7.0 from 1.0 mg/ml solution in 50 mM sodium phosphate pH 7.0 for 1 h. Height range is 10 nm.

Thus, we can demonstrate that films of $PB_{290}$-*b*-$PDMAEMA_{240}$ on hydrophobic substrates like HOPG are formed, indicating good adhesion of this diblock copolymer to carbon materials. It is worthy to note that a similar $PB_{250}$-*b*-$PDMAEMA_{507}$ diblock copolymer with a PB

block of comparable length but having about 2-times longer PDMAEMA block forms more or less condensed films (however still having holes due to dewetting) on HOPG only at high pH, such as pH 10.[39] This might manifest the importance of the hydrophobic-hydrophilic balance of the amphiphilic diblock copolymers for the topographical features of their films on hydrophobic substrates.

Next, we examined how $PB_{290}$-*b*-$PDMAEMA_{240}$ films can effectively bind myoglobin. We applied quartz crystal microbalance with dissipation monitoring (QCM-D) that allows simultaneous in situ measurements of a layer resonance frequency, *f*, and dissipation, *D,* at several overtones of the fundamental frequency that both are sensitive to the mass of adsorbed material and its viscoelastic properties. The change in frequency ($\Delta f$) and the change in dissipation ($\Delta D$) during each adsorption stage obtained at overtone numbers of n = 3, 5, 7, 9, and 11 were recorded as a function of time. To be able to make some quantitative comparisons, frequency shifts were calculated for the 7th overtone taking the difference in the values of $f_7$ before and after component adsorption. To a first approximation this can be interpreted as values proportional to the masses of hydrated films adsorbed onto the quartz crystal.

In our QCM-D experiments, we examined the interaction of sk-Mb with naked gold-coated quartz crystals or with the same samples pre-modified with $PB_{290}$-*b*-$PDMAEMA_{240}$ films deposited at different concentrations of the diblock copolymer. Each experiment was carried out in a flow-through QCM cell and was started from baseline recording for the corresponding buffer, followed by the adsorption experiment. Then, a rinsing step was performed in order to confirm that both the changes in *f* and *D* are not the result of variations in the solution properties, such as density and viscosity.

As was found (Fig. 4A), a direct adsorption of sk-Mb onto a bare gold-coated quartz crystal leads to ca 23 Hz decrease in *f* and a small increase in *D* for about 20 min adsorption. This observation is in a good agreement with others who examined Mb interaction with gold substrates covered by citrate.[48] This behavior points towards a very thin film of sk-Mb formed

(which globules has slight negative charge at pH 7.4 according to its IEP of about 7.0[48] and being additionally screened by counterions from 100 mM potassium phosphate with 50 mM NaCl) on a similarly charged gold substrates (which are charged slightly negatively at neutral pHs according to the data on streaming potential[49]).
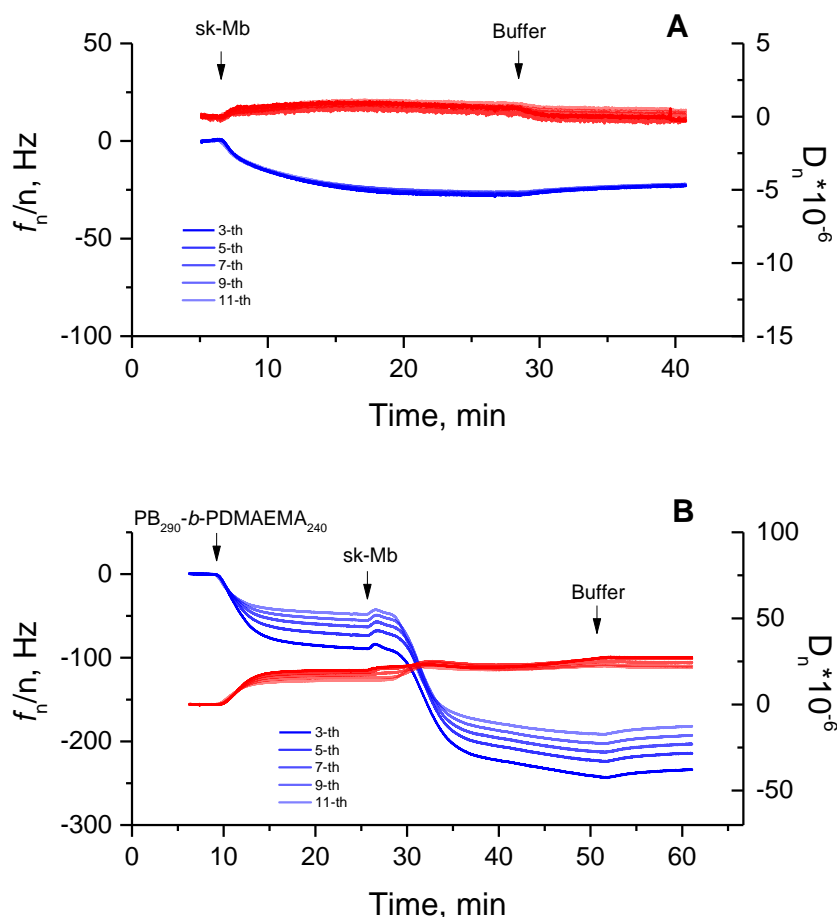


Fig. 4. Frequency $f_n/n$ (normalized to overtone number n), and dissipation, $D_n$ shifts for gold-coated quartz crystal upon the interaction with sk-Mb (A) or with $PB_{290}$-$b$-$PDMAEMA_{240}$ micelles and sk-Mb, subsequently (B). Conditions: $PB_{290}$-$b$-$PDMAEMA_{240}$ was adsorbed from 1 mg/ml solution in 100 mM potassium phosphate with 50 mM NaCl of pH 8.2; sk-Mb was adsorbed from 100 μM solution in 100 mM potassium phosphate with 50 mM NaCl of pH 7.4.

In contrast, $PB_{290}$-$b$-$PDMAEMA_{240}$ can be easily adsorbed onto the gold-coated quartz crystals. A representative QCM-D experiment using a 1 mg/ml solution of $PB_{290}$-$b$-$PDMAEMA_{240}$ is shown in Fig. 4B. One can clearly see that the interaction with $PB_{290}$-$b$-$PDMAEMA_{240}$ results in a fast (not longer than 10 min) and pronounced decrease of $f$ and an increase of $D$ with the spreading of overtones, which denotes that the mass deposited onto the crystal surface exhibits viscoelastic properties. No notable increase in the shifts of $\Delta f$ values is

observed with increasing concentration of PB$_{290}$-$b$-PDMAEMA$_{240}$ from 0.5 mg/ml to 2 mg/ml

that can be a sign of saturation taking place in this PB$_{290}$-$b$-PDMAEMA$_{240}$ concentration range

(Table 1).

Table 1. Frequency shifts ($\Delta f_7$) for films of PB$_{290}$-$b$-PDMAEMA$_{240}$ or sk-Mb fabricated at different concentrations of diblock copolymer upon the subsequent interactions of gold-coated quartz crystal with PB$_{290}$-$b$-PDMAEMA$_{240}$ and sk-Mb.

| System | | Diblock copolymer adsorption ($\Delta f_7$, Hz) | sk-Mb adsorption ($\Delta f_7$, Hz) |
|---|---|---|---|
| Bare gold-coated quartz crystal | | - | 23±1 |
| Diblock copolymer Concentration | 0.5 mg/ml | 50±16 | 194±18 |
| | 1.0 mg/ml | 64±8 | 188±21 |
| | 2.0 mg/ml | 67±11 | 197±26 |

Conditions: PB$_{290}$-$b$-PDMAEMA$_{240}$ was adsorbed from solutions of different concentration in 100 mM potassium phosphate with 50 mM NaCl of pH 8.2; sk-Mb was adsorbed from 100 μM solution in 100 mM potassium phosphate with 50 mM NaCl of pH 7.4.

Thereafter, the interaction of sk-Mb with the films of PB$_{290}$-$b$-PDMAEMA$_{240}$ deposited

at different concentrations was examined. One can see facilitated adsorption of sk-Mb onto the

pre-adsorbed diblock copolymer film (Fig. 4B). This enhanced adsorption of sk-Mb might be

caused by the electrostatically driven interaction between positively charged (at this specified pH

condition of pH 7.4) PDMAEMA and slightly negatively charged sk-Mb (isoelectric point of

7.0), which can be superimposed on hydrophobic interactions reported for myoglobin adsorption

in[48] and possible hydrogen bonding. All this results in a considerable increase in the shifts of $\Delta f_7$,

which were found to be about 8-9-fold higher in comparison to sk-Mb interactions with bare

quartz crystal (Table 1).

By QCM-D, we can therefore demonstrate the pronounced interaction of sk-Mb with pre-

adsorbed PB$_{290}$-$b$-PDMAEMA$_{240}$ films upon subsequent adsorption of both components onto the

solid interface. Together with good adhesion of this diblock copolymer to carbon materials

shown by AFM experiments (Fig. 3), one can expect that this material is well-suited as binding

agent for composites comprising MWCNTs and biomolecules like Mb.

Another important aspect is the biocompatibility of the guest polymeric matrix to the host

biomaterial. This is important as the resultant biosensor should be suitable for long-term use in

complex biological environments, such as blood, plasma, serum, and/or as implant.[41, 42]

Biocompatibility of $PB_{290}$-$b$-$PDMAEMA_{240}$ with respect to sk-Mb was examined by studying the

spectral properties of Mb after its integration into a diblock copolymer film adsorbed on a

surface of polyvinylchloride plates similarly to the method described elsewhere.[17, 50-52] The

experiments show no significant change in the UV-Vis spectrum for sk-Mb and, more

specifically, no change in the position of the characteristic Soret absorbance band ($\lambda_{max}$ = 409

nm) in comparison with the Mb control sample (Fig. 5). Therefore, we assume that the

incorporation of Mb into $PB_{290}$-$b$-$PDMAEMA_{240}$ films does not change the tertiary structure of
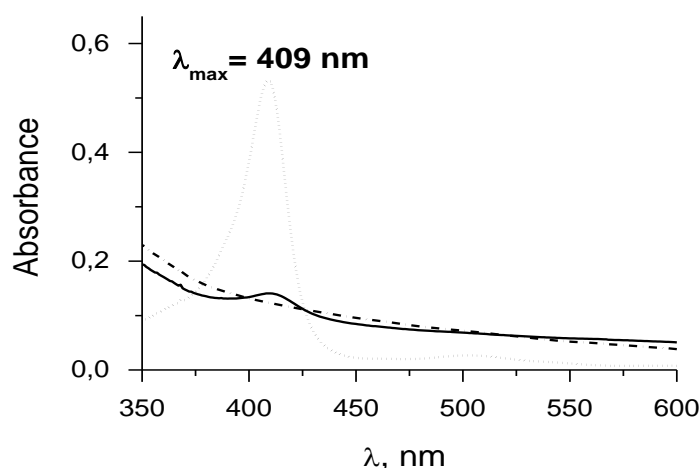
at least some Mb.



Fig 5. UV-Vis absorption spectra of sk-Mb incorporated into $PB_{290}$-$b$-$PDMAEMA_{240}$ films (solid line); sk-Mb in solution in a concentration of 25 µM in 100 mM potassium phosphate with 50 mM NaCl of pH 7.4 (dot line) used as positive control; and absorption spectra of a $PB_{290}$-$b$-$PDMAEMA_{240}$ film (dash-dot line) used as negative control.

To have an impression how the interactions in MWCNTs/$PB_{290}$-$b$-$PDMAEMA_{240}$/sk-Mb

nanocomposite correlate with its microstructure and influence the performance of the resulting

biosensor, we used a combination of TEM and SEM techniques to visualize the surface

morphology of subsequently drop casted MWCNTs, $PB_{290}$-$b$-$PDMAEMA_{240}$ and sk-Mb. As can

be seen in Figures 6A, 6B, mostly thin bundles of MWNTs are observed upon drop-casting of

MWCNTs suspension from chloroform. Upon the addition of $PB_{290}$-$b$-$PDMAEMA_{240}$, MWCNTs are still well recognizable (Fig. 6D), although one can mention a decrease of sharpness of TEM image due to electron beam scattering on $PB_{290}$-$b$-$PDMAEMA_{240}$ film (Fig. 6C). Similarly to above discussed AFM data, no individual micelles are observed after $PB_{290}$-$b$-$PDMAEMA_{240}$ deposition, thus suggesting rather uniform distribution of diblock copolymer on surfaces of MWCNTs as a thing film. When sk-Mb is finally introduced, the morphology of MWCNTs/$PB_{290}$-$b$-$PDMAEMA_{240}$/sk-Mb sample demonstrates no additional changes (Fig. 6F), whereas one can see further decrease of the sharpness of TEM image (Fig. 6E) due to further increase in MWCNTs/$PB_{290}$-$b$-$PDMAEMA_{240}$/sk-Mb film thickness. The latter is also pointing to uniform distribution of sk-Mb on surfaces of MWCNTs covered by $PB_{290}$-$b$-$PDMAEMA_{240}$. Such uniform morphology seems to suggest mutual compatibility among the components of the MWCNTs/$PB_{290}$-$b$-$PDMAEMA_{240}$/sk-Mb construct and is expected to provide advantages for Mb electrochemistry.
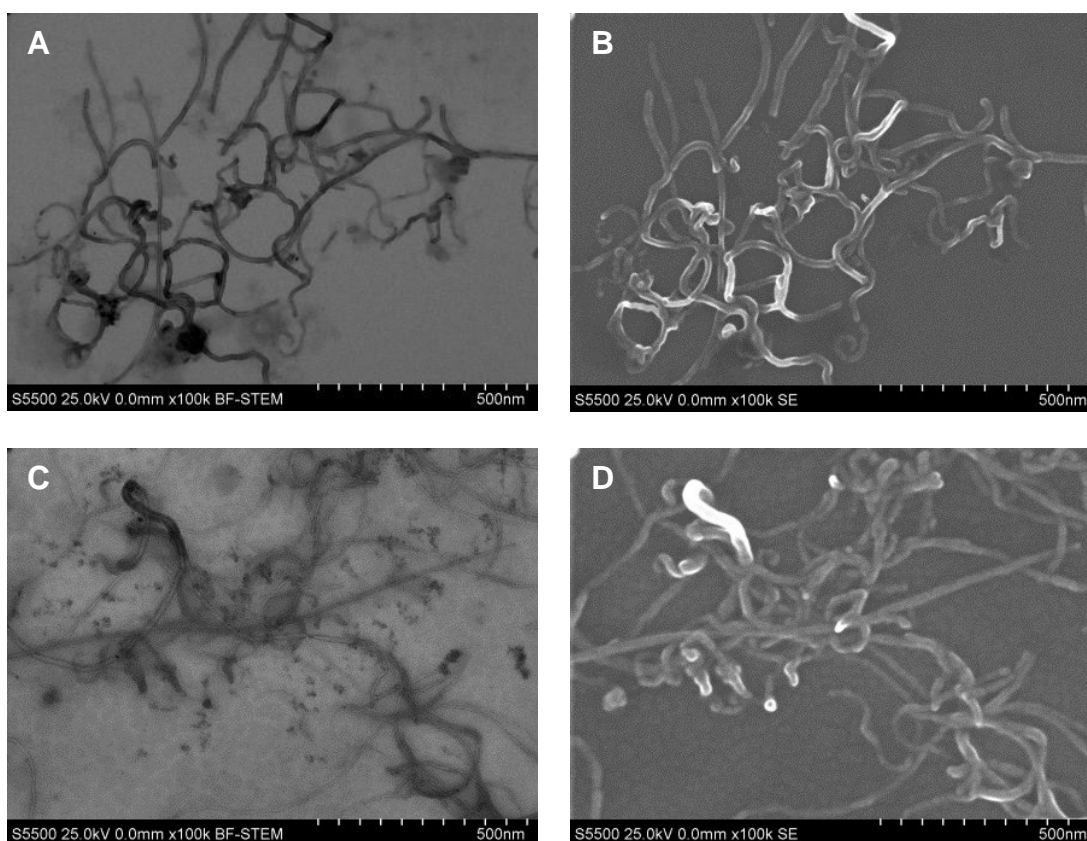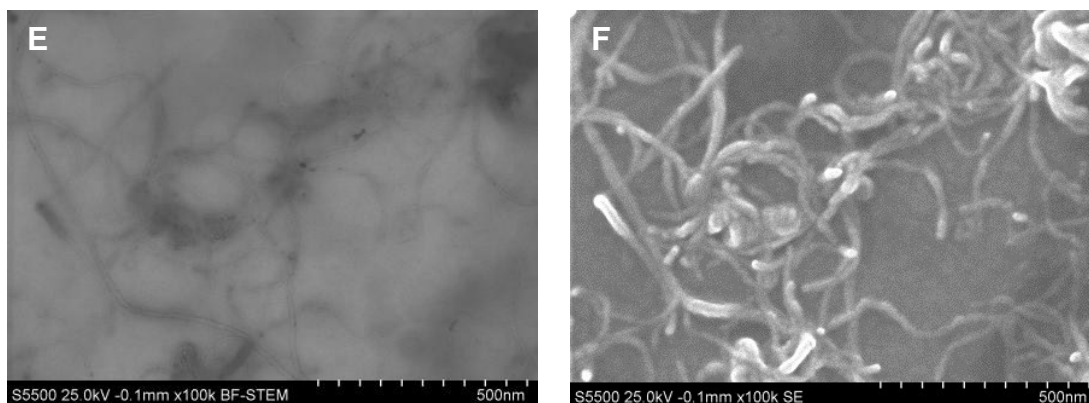
Fig. 6. BF-STEM images (A, C, E) and SE-SEM images (B, D, F) for the same sample after subsequent addition of MWCNTs in chloroform (A, B), $PB_{290}$-*b*-$PDMAEMA_{240}$ (C, D), and sk-Mb (E, F).

## 3. Direct electrochemistry of myoglobin by SPE/$PB_{290}$-*b*-$PDMAEMA_{240}$/sk-Mb or SPE/MWCNTs/$PB_{290}$-*b*-$PDMAEMA_{240}$/sk-Mb electrodes

The adsorption of sk-Mb onto the bare SPE (SPE/sk-Mb system) does not lead to observable direct electron transfer processes of Mb as studied by CV or SWV. However, integration of sk-Mb into $PB_{290}$-*b*-$PDMAEMA_{240}$ films leads to such processes in accordance with scheme[53]:

$$Mb–Fe(III) + e^- + H^+ \leftrightarrow Mb–Fe(II)$$

$$Mb–Fe(II) + O_2 \rightarrow [Mb–Fe(II)O_2] \rightarrow Mb–Fe(III) + O_2^-$$
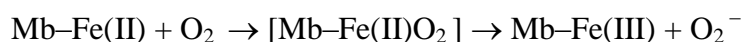
While the CV of SPE/$PB_{290}$-*b*-$PDMAEMA_{240}$/sk-Mb electrodes demonstrates only a slight and indistinct reductive peak ($E_{CV}$ of about –420 ~ –450 mV) (Fig. 7A), the SWV of SPE/$PB_{290}$-*b*-$PDMAEMA_{240}$/sk-Mb electrodes shows more clear reductive peaks at the same potential (Fig. 7, B). Our previous data on direct electron transfer of Mb incorporated in DDAB film[53] exhibited a reductive peak at the position ($E_{SWV} = -250$ mV) that corresponds to the heme protein reduction. Comparing to the DDAB electrode, one can see that the reductive potential for the herein presented SPE/$PB_{290}$-*b*-$PDMAEMA_{240}$/sk-Mb system shifts to more negative values, corresponding to an increase in overpotential. This also points out to a complication of the direct electron transfer to heme iron.

21

For improvement of the electron transfer properties and electroanalytical characteristics, we further modified the SPEs by applying a MWCNTs suspension in a volatile solvent (chloroform). The subsequent drop-casting of $PB_{290}$-$b$-$PDMAEMA_{240}$ promotes both (i) fixing of MWCNTs on a surface of graphite electrodes preventing leakage of MWCNTs and (ii) effective integration of a heme protein for carrying out the electroanalysis. Besides, the diblock copolymer films might protect the carbon nanomaterial from direct contact with biological fluids. The latter can be interesting and important when developing an implantable sensor system, taking into account the absence of reliable data on long-term exposure of organisms to carbon nanotubes.
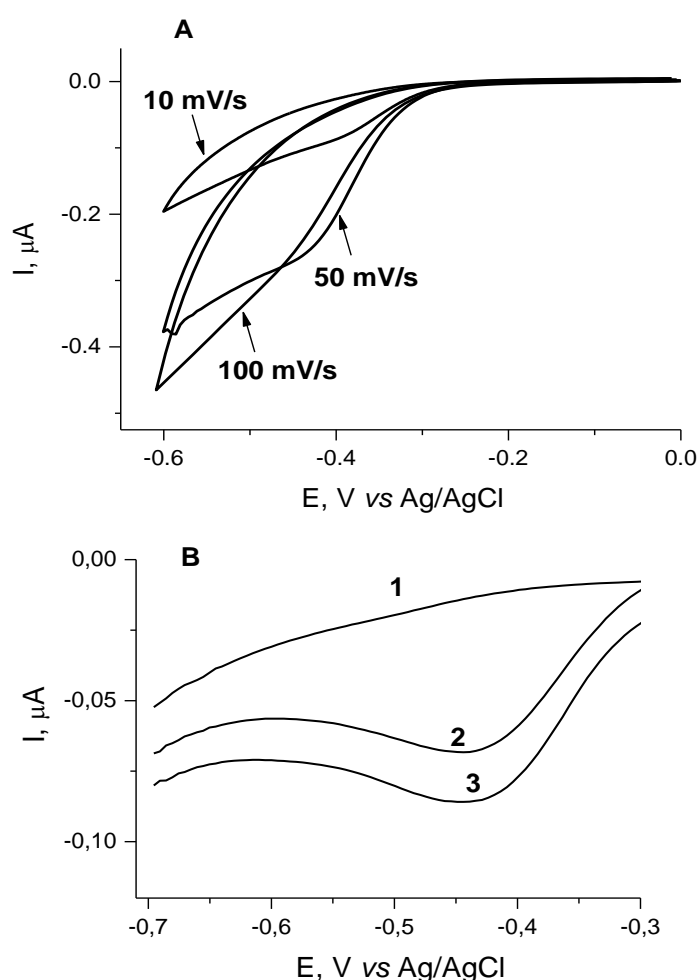


Fig. 7. CVs (A) of SPE/$PB_{290}$-$b$-$PDMAEMA_{240}$ (0.5 mg/ml)/sk-Mb electrodes at scan rates 10, 50, and 100 mV/s in oxygenated 100 mM potassium phosphate buffer with 50 mM NaCl of pH 7.4 and reductive SWVs (B) of SPE/$PB_{290}$-$b$-$PDMAEMA_{240}$ (2.0 mg/ml) (1), SPE/$PB_{290}$-$b$-$PDMAEMA_{240}$ (2.0 mg/ml)/sk-Mb (2), SPE/$PB_{290}$-$b$-$PDMAEMA_{240}$ (0.5 mg/ml)/sk-Mb (3), in oxygenated 100 mM potassium phosphate buffer with 50 mM NaCl of pH 7.4. Conditions for SWV: scan rate 50 mV/s, amplitude 20 mV, step height 5 mV; frequency 10 Hz.

Fig. 8 shows CV and reductive SWV of the SPE/MWCNTs/PB$_{290}$-*b*-PDMAEMA$_{240}$/sk-Mb constructs. A well-defined redox peaks shape is observed at E$_{CV}$ ~ −200 mV in CVs with different scan rates in the range of 10-100 mV/s (Fig. 8A). As seen in the inset of Fig. 8, the anodic and cathodic peak current for incorporated Mb exhibit a linear relationship with the scan rate in the range of 10-100 mV/s, indicating phenomenon of protein film voltammetry and a typical surface-controlled electrode process.[54, 55] The surface coverage $\Gamma_0$, (mol cm$^{-2}$) of electroactive Mb in the MWCNTs/PB$_{290}$-*b*-PDMAEMA$_{240}$ film could be expressed using Faraday's Law according to the following formula: $Q = nFA\Gamma_0$, where F is the Faraday's constant (96484.6 C/mol), n is the number of electrons transferred, A is the surface area of the electrode (here 0.0314 cm$^2$), Q (C) is the quantity of charge. Therefore, the average value of $\Gamma_0$ is calculated as $9.9\pm1.2\times10^{-10}$ mol/cm$^2$. Compared with the theoretic value of surface concentration of sk-Mb ($6.4\times10^{-9}$ mol/cm$^2$), there was about 16.0±2.1% of total amount of sk-Mb deposited on the electrode involved in the electron-transfer (electroactive Mb). According to the model of Laviron,[56] the electron transfer rate constant (k$_s$) value between sk-Mb and SPE/MWCNTs/PB$_{290}$-*b*-PDMAEMA$_{240}$ electrode is estimated to be 0.30±0.04 s$^{-1}$. Similarly to CV, the clear reductive peaks were measured by SWV both for SPE/MWCNTs/sk-Mb and for SPE/MWCNTs/PB$_{290}$-*b*-PDMAEMA$_{240}$/sk-Mb systems (Fig. 8B).

Thus, the modification of SPE by MWCNTs leads to a great (50-80-fold) improvement of electron transport properties and facilitates direct electron transfer of Mb. Moreover, the presence of PB$_{290}$-*b*-PDMAEMA$_{240}$ do not induce any blocking of direct electron transfer process, but contrary has obvious positive effects, resulting in notable concentration-dependent increase in cathodic peak area and decrease in redox potential (Fig. 8B, Table 2). Thus, up to about 180-fold cumulative effect of MWCNTs and PB$_{290}$-*b*-PDMAEMA$_{240}$ (2 mg/ml) was achieved in an increase of the reductive current of sk-Mb incorporated into the SPE/MWCNTs/PB$_{290}$-*b*-PDMAEMA$_{240}$ matrix in comparison to samples without MWCNTs.
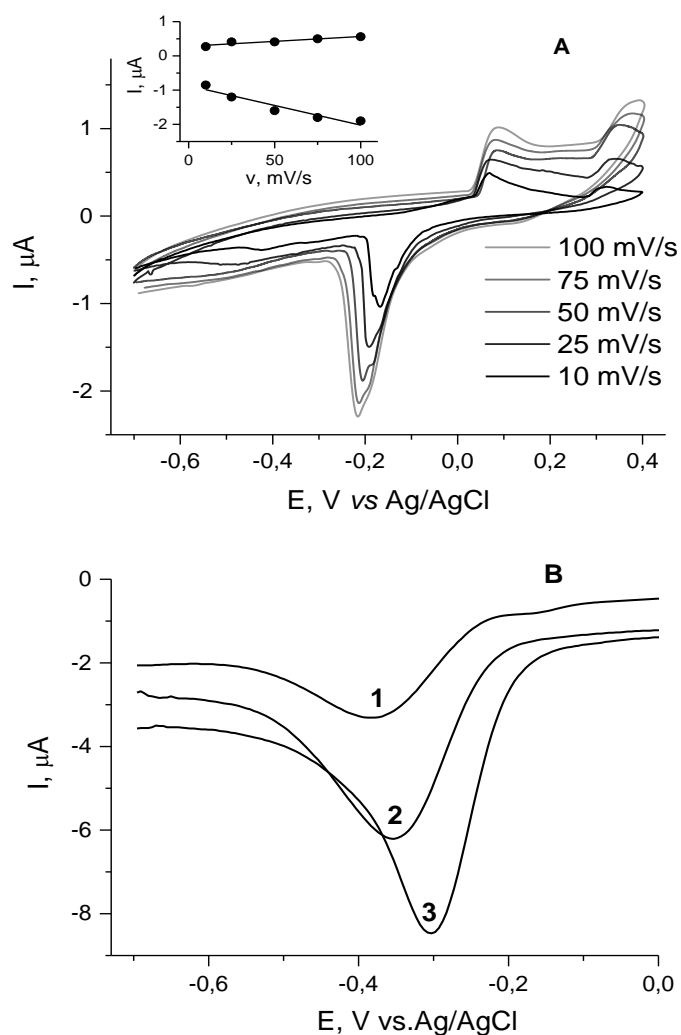
Fig. 8. (A) CVs of SPE/MWCNTs/PB$_{290}$-$b$-PDMAEMA$_{240}$ (0.5 mg/ml)/sk-Mb electrodes at different scan rates in deoxygenated 100 mM potassium phosphate buffer with 50 mM NaCl of pH 7.4. Insert: plot of the peak current I against the scan rate $v$. (B) Reductive SWVs of SPE/MWCNTs/sk-Mb (1), SPE/MWCNTs/PB$_{290}$-$b$-PDMAEMA$_{240}$ (0.5 mg/ml)/sk-Mb (2), SPE/MWCNTs/PB$_{290}$-$b$-PDMAEMA$_{240}$ (2.0 mg/ml)/sk-Mb (3) in oxygenated 100 mM potassium phosphate buffer with 50 mM NaCl of pH 7.4. Conditions for SWV: scan rate 50 mV/s, amplitude 20 mV, step height 5 mV; frequency 10 Hz.

Table 2. Comparative quantitative electrochemical characteristics of electrodes according to reductive SWV (oxygenated 100 mM potassium phosphate buffer with 50 mM NaCl of pH 7.4)

| Electrode | Cathodic peak area ×10$^{-9}$ | Peak potential, mV |
|---|---|---|
| SPE/sk-Mb | ND[*] | ND |
| SPE/PB$_{290}$-$b$-PDMAEMA$_{240}$ (0.5÷2.0 mg/ml) | ND | ND |
| SPE/PB$_{290}$-$b$-PDMAEMA$_{240}$ (0.5 mg/ml)/sk-Mb | 7.66±0.70 | -427±3 |
| SPE/PB$_{290}$-$b$-PDMAEMA$_{240}$ (2.0 mg/ml)/sk-Mb | 5.64±1.68 | -455±25 |
| SPE/MWCNTs/PB$_{290}$-$b$-PDMAEMA$_{240}$ (0.5÷2.0 mg/ml) | ND | ND |

| | | |
|---|---|---|
| SPE/MWCNTs/sk-Mb | 420±35 | -356±18 |
| SPE/MWCNTs/PB$_{290}$-$b$-PDMAEMA$_{240}$ (0.5 mg/ml)/sk-Mb | 709±10 | -343±10 |
| SPE/MWCNTs/PB$_{290}$-$b$-PDMAEMA$_{240}$ (2.0 mg/ml)/sk-Mb | 1039±37 | -308±7 |

$^{*)}$ ND – not detected

## 4. Application for cardiac myoglobin (c-Mb) detection in human plasma

As appears from Fig. 8B and Table 1, SPEs modified by MWCNTs/PB$_{290}$-$b$-PDMAEMA$_{240}$ (2.0 mg/ml) shows the highest reductive current for incorporated sk-Mb. Taking into account complete primary structure identity of cardiac and skeletal forms of this heme protein according to UniProtKB[57] (protein code P02144), we assumed that our results obtained for sk-Mb (as a model protein) might be also expanded to c-Mb.

In this section, we will demonstrate that the above described MWCNTs/PB$_{290}$-$b$-PDMAEMA$_{240}$ nanocomposites can be used for the design of advanced biosensor setups for potential applications for the analysis of clinically relevant systems, specifically for the detection of cardiac Mb (c-Mb) in human plasma. We demonstrate the applicability of new nanocomposite materials for c-Mb assays, while the analytical performance, optimization, and comparison to current standard myoglobin assays were already described in previous work for different biosensor setups for c-Mb.[58-61]

To increase selectivity and specificity of the c-Mb assay we apply known approach, when the SPE/MWCNTs/PB$_{290}$-$b$-PDMAEMA$_{240}$ constructs were further pre-modified by antibodies to cardiac human myoglobin (anti-myoglobin, Ab$^{Mb}$), which will specifically bind c-Mb to be analyzed (Ab$^{Mb}$-c-Mb coupling).[58-60] By integrating anti-myoglobin antibodies into the nanocomposite, myoglobin from blood samples will specifically binds with Ab$^{Mb}$ and forced into the layer where quantified via the changes in the electrical properties. To acheive this, Ab$^{Mb}$ were immobilized onto the SPE/MWCNTs/PB$_{290}$-$b$-PDMAEMA$_{240}$ (2 mg/ml) electrode by drop-casting of an Ab$^{Mb}$ solution with following overnight incubation/drying at +4 $^{o}$C, assuming that

25

integration of Ab$^{Mb}$ into the MWCNTs/PB$_{290}$-*b*-PDMAEMA$_{240}$ nanocomposites is governed by comparable forces as in the case of Mb.

For c-Mb determination, we used plasma of both a healthy donor (HD, 43 ng/ml of myoglobin) and a patient with AMI (1600 ng/ml of myoglobin). The concentration of c-Mb in plasma was estimated independently with the bench-top lateral flow RAMP® (Response Biomedical Corp) immunoassay as described earlier.[41, 42, 58, 59, 61]

Human plasma was analyzed using electrochemical SPE/MWCNTs/PB$_{290}$-*b*-PDMAEMA$_{240}$/Ab$^{Mb}$ immunosensors by recording their CVs after 15-min incubation with plasma samples. As can be seen from Fig. 9, a strong dependence of cathodic peak height of CV (E = −216 mV) from the concentration of c-Mb is observed, while the control electrode with non-electroactive Ab$^{Mb}$ does not exhibit a peak in the field of a heme protein. This result indicates both (i) the successive fixation of antibodies on the SPE/MWCNTs/PB$_{290}$-*b*-PDMAEMA$_{240}$ nanocomposite electrode (otherwise the response from Mb would not be as high and pronounced as we observe) and (ii) the distinct possibility of sensitive and fast assay of c-Mb with this setup due to high specific interactions of Mb with Ab$^{Mb}$.
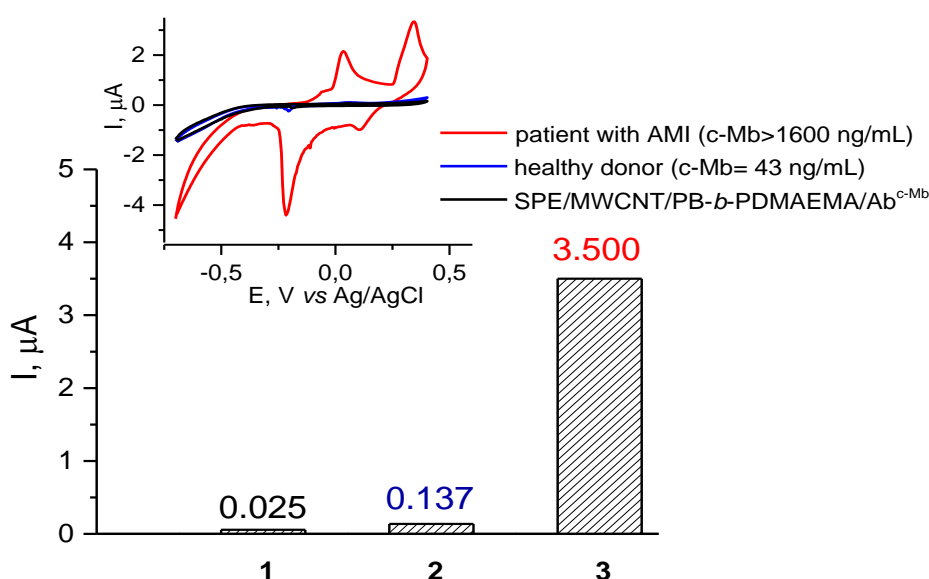


Fig. 9. Reductive cathodic peak height of CV for MWCNTs/PB$_{290}$-*b*-PDMAEMA$_{240}$ (2 mg/ml)/Ab$^{Mb}$ (1), MWCNTs/PB$_{290}$-*b*-PDMAEMA$_{240}$ (2 mg/ml)/Ab$^{Mb}$ after 15-min incubation with plasma of healthy donor (43 ng/ml of c-MB) (2), MWCNTs/PB$_{290}$-*b*-PDMAEMA$_{240}$ (2 mg/ml)/Ab$^{Mb}$ after 15-min incubation with plasma of patient with AMI (1600 ng/ml of c-MB)

(3). Insert: Corresponding CVs at scan rate 50 mV/s, in oxygenated 100 mM potassium phosphate with 50 mM NaCl of pH 7.4. The concentration of cardiac myoglobin in plasma samples was determined independently by bench-top lateral flow RAMP® (Response Biomedical Corp) immunoassay.

Comparing these new results with our previous data on quantitative myoglobin detection in plasma samples, we emphasize that in our former biosensor setups only highly-sensitive voltammetric analysis (square wave voltammetry (SWV)) was able to register AMI samples using electrodes modified with gold nanoparticles/didodecyldimethylammonium bromide (AuNP/DDAB).[58, 60] Indeed, the cathodic peak area of SWV for SPE/DDAB/AuNps/Mb (normalized to the Mb concentration and to the surface area of electrode), corresponded to 9.1 $A*V$ /($\mu M*cm^2$).[58] Values obtained for SPE/MWCNTs/Mb, SPE/MWCNTs/PB$_{290}$-*b*-PDMAEMA$_{240}$ (0.5 mg/ml)/Mb, and SPE/ MWCNTs/PB$_{290}$-*b*-PDMAEMA$_{240}$ (2.0 mg/ml)/Mb were 12.8, 21.7, and 31.8 $A*V$ /($\mu M*cm^2$), respectively. The herein developed approach therefore seems highly promising for quantitative detection of c-Mb. The herein developed MWCNT/PB$_{290}$-*b*-PDMAEMA$_{240}$/Ab$^{Mb}$ immunosensors demonstrate higher sensitivity with respect to c-Mb, thus allowing to register HD and AMI samples using only CV with clear reduction peaks corresponding to the electrochemical reduction of Mb. The sensitivity of this biosensor system is enough to cover the whole range of c-Mb starting from normal physiological concentration of human cardiac myoglobin (10-100 ng/ml; 0.56 nM − 5.6 nM) to c-Mb levels in patients with AMI (100-1780 ng/ml; 5.6 nM - 100 nM).

## Conclusions

We developed a facile electrochemical method for the detection of myoglobin based on the electroactivity of Fe(III)/Fe(II)-heme, the direct detection of specific interactions between anti-myoglobin and heme protein, as well as the electro catalytic properties of reduced myoglobin with respect to oxygen. This was realized by specific electron transport properties of MWCNTs/PB$_{290}$-*b*-PDMAEMA$_{240}$ nanocomposites along with an unaltered state of (at least

significant parts) Mb after incorporation into the diblock copolymer matrix. Such materials were found to be promising as highly-sensitive biospecific recognition systems for quantitative c-Mb assays. The proposed system in our opinion is an ambitious alternative to known detection systems of c-Mb as a very early marker of AMI. Obviously, the application of the herein described MWCNTs/PB$_{290}$-$b$-PDMAEMA$_{240}$ nanocomposites is not restricted exclusively to heme-containing proteins. We assume that this nanocomposite material can be readily extended to other oxidative enzymes for the detection of various clinically important target molecules and, hence, can be used to develop convenient and robust biosensors for practical applications.

## Acknowledgements

## References

1. V. V. Shumyantseva, E. V. Suprun, T. V. Bulko, Y. M. Chalenko and A.I. Archakov, Electrochemical Sensor Systems for Medicine. In *Nanomedicine in Diagnostics*; N. Rozlosnik, N., Ed.; Science Publisher: Enfield, USA, 2012; Part 4. pp 68-95.
2. V. V. Shumyantseva, T. V. Bulko, E. V. Suprun, Y. M. Chalenko, M. Y. Vagin, Y. O. Rudakov, M. A. Shatskaya and A. I. Archakov, *Biochimica Et Biophysica Acta-Proteins and Proteomics*, 2011, **1814**, 94-101.
3. Allender, S.; Scarborough, P.; Peto, V.; Rayner, M.; Leal, J.; Luengo-Fernandez, R.; Gra, A., *European cardiovascular disease statistics*; European Heart Network: Brussels; 2008.
4. http://www.gks.ru.
5. H. C. Vaidya, *Lab. Med.*, 1992, **23**, 306-310.
6. B. McDonnell, S. Hearty, P. Leonard and R. O'Kennedy, *Clinical Biochemistry*, 2009, **42**, 549-561.
7. W. J. Zhang and G. X. Li, *Analytical Sciences*, 2004, **20**, 603-609.
8. B. Krajewska, *Enzyme and Microbial Technology*, 2004, **35**, 126-139.
9. L. V. Sigolaeva, S. Y. Gladyr, A. P. H. Gelissen, O. Mergel, D. V. Pergushov, I. N. Kurochkin, F. A. Plamper and W. Richtering, *Biomacromolecules*, 2014, **15**, 3735-3745.
10. L. V. Sigolaeva, G. V. Dubacheva, M. V. Porus, A. V. Eremenko, E. V. Rudakova, G. F. Makhaeva, R. J. Richardson and I. N. Kurochkin, *Analytical Methods*, 2013, **5**, 3872-3879.

11. L. Sigolaeva, G. Makhaeva, E. Rudakova, N. Boltneva, M. Porus, G. Dubacheva, A. Eremenko, I. Kurochkin and R. J. Richardson, *Chemico-Biological Interactions*, 2010, **187**, 312-317.

12. D. Buenger, F. Topuz and J. Groll, *Progress in Polymer Science*, 2012, **37**, 1678-1719.

13. J. R. Siqueira, Jr., L. Caseli, F. N. Crespilho, V. Zucolotto and O. N. Oliveira, Jr., *Biosensors & Bioelectronics*, 2010, **25**, 1254-1263.

14. F. R. R. Teles and L. R. Fonseca, *Materials Science & Engineering C-Biomimetic and Supramolecular Systems*, 2008, **28**, 1530-1543.

15. A. Chen and S. Chatterjee, *Chemical Society Reviews*, 2013, **42**, 5425-5438.

16. J. F. Rusling and A. E. F. Nassar, *Journal of the American Chemical Society*, 1993, **115**, 11891-11897.

17. P. M. Guto and J. F. Rusling, *Electrochemistry Communications*, 2006, **8**, 455-459.

18. V. Shumyantseva, E. Suprun, T. Bulko and A. Archakov, *Electroanalysis*, 2009, **21**, 530-535.

19. T. Yin and W. Qin, *Trac-Trends in Analytical Chemistry*, 2013, **51**, 79-86.

20. Y. Lv, T. Tan and F. Svec, *Biotechnology Advances*, 2013, **31**, 1172-1186.

21. J. Wang and Y. Lin, *Trac-Trends in Analytical Chemistry*, 2008, **27**, 619-626.

22. S. Carrara, V. V. Shumyantseva, A. I. Archakov and B. Samori, *Biosensors & Bioelectronics*, 2008, **24**, 148-150.

23. C. I. L. Justino, T. A. P. Rocha-Santos and A. C. Duarte, *Trac-Trends in Analytical Chemistry*, 2013, **45**, 24-36.

24. S. Carrara, C. Baj-Rossi, C. Boero and G. De Micheli, *Electrochimica Acta*, 2014, **128**, 102-112.

25. C. Hu and S. Hu, *Encyclopedia of Nanotechnology, Vols 1 and 2*, 2009, 749-808.

26. S. K. Smart, A. I. Cassady, G. Q. Lu and D. J. Martin, *Carbon*, 2006, **44**, 1034-1047.

27. X. Wang and Z. Liu, *Chinese Science Bulletin*, 2012, **57**, 167-180.

28. S. Utsel, A. Carlmark, T. Pettersson, M. Bergstrom, E. E. Malmstrom and L. Wagberg, *European Polymer Journal*, 2012, **48**, 1195-1204.

29. S. Förster, V. Abetz and A. H. E. Müller, *Polyelectrolytes with Defined Molecular Architecture Ii*, 2004, **166**, 173-210.

30. K. Emoto, M. Iijima, Y. Nagasaki and K. Kataoka, *Journal of the American Chemical Society*, 2000, **122**, 2653-2654.

31. G. B. Webber, E. J. Wanless, S. P. Armes, F. L. Baines and S. Biggs, *Langmuir*, 2001, **17**, 5551-5561.

32. M. R. Talingting, Y. H. Ma, C. Simmons and S. E. Webber, *Langmuir*, 2000, **16**, 862-865.

33. V. M. De Cupere, J. F. Gohy, R. Jérôme and P. G. Rouxhet, *J Colloid Interf Sci*, 2004, **271**, 60-68.

34. K. Sakai, E. G. Smith, G. B. Webber, M. Baker, E. J. Wanless, V. Bütün, S. P. Armes and S. Biggs, *J Colloid Interf Sci*, 2007, **314**, 381-388.

35. K. Sakai, E. G. Smith, G. B. Webber, M. Baker, E. J. Wanless, V. Bütün, S. P. Armes and S. Biggs, *Langmuir*, 2006, **22**, 8435-8442.

36. Z. Wang, J. Yi and S. Yang, *Sensors and Actuators B-Chemical*, 2013, **176**, 211-216.

37. S. Jia, J. Fei, J. Deng, Y. Cai and J. Li, *Sensors and Actuators B-Chemical*, 2009, **138**, 244-250.

38. L. V. Sigolaeva, U. Günther, D. V. Pergushov, S. Y. Gladyr, I. N. Kurochkin and F. H. Schacher, *Macromolecular Bioscience*, 2014, **14**, 1039-1051.

39. L. V. Sigolaeva, D. V. Pergushov, C. V. Synatschke, A. Wolf, I. Dewald, I. N. Kurochkin, A. Fery and A. H. E. Müller, *Soft Matter*, 2013, **9**, 2858-2868.

40. M. S. Gromova, L. V. Sigolaeva, M. A. Fastovets, E. G. Evtushenko, I. A. Babin, D. V. Pergushov, S. V. Amitonov, A. V. Eremenko and I. N. Kurochkin, *Soft Matter*, 2011, **7**, 7404-7409.

41. A. Turner, *Trends in Biotechnology*, 2013, **31**, 119-120.
42. C. N. Kotanen, F. G. Moussy, S. Carrara and A. Guiseppi-Elie, *Biosensors & Bioelectronics*, 2012, **35**, 14-26.
43. F. Schacher, M. Müllner, H. Schmalz and A. H. E. Müller, *Macromolecular Chemistry and Physics*, 2009, **210**, 256-262.
44. F. A. Plamper, M. Ruppel, A. Schmalz, O. Borisov, M. Ballauff and A. H. E. Müller, *Macromolecules*, 2007, **40**, 8361-8366.
45. M. Burkhardt, N. Martinez-Castro, S. Tea, M. Drechsler, I. Babin, I. Grishagin, R. Schweins, D. V. Pergushov, M. Gradzielski, A. B. Zezin and A. H. E. Müller, *Langmuir*, 2007, **23**, 12864-12874.
46. A. Schallon, C. V. Synatschke, D. V. Pergushov, V. Jérôme, A. H. E. Müller and R. Freitag, *Langmuir*, 2011, **27**, 12042-12051.
47. I. Choi, R. Suntivich, F. A. Plamper, C. V. Synatschke, A. H. E. Müller and V. V. Tsukruk, *Journal of the American Chemical Society*, 2011, **133**, 9592-9606.
48. W. R. Glomm, O. Halskau, Jr., A.-M. D. Hanneseth and S. Volden, *Journal of Physical Chemistry B*, 2007, **111**, 14329-14345.
49. A. M. Gallardo-Moreno, V. Vadillo-Rodriguez, J. Perera-Nunez, J. M. Bruque and M. Luisa Gonzalez-Martin, *Physical Chemistry Chemical Physics*, 2012, **14**, 9758-9767.
50. N. Sultana, J. B. Schenkman and J. F. Rusling, *Electroanalysis*, 2007, **19**, 2499-2506.
51. Z. Zhang, A. E. F. Nassar, Z. Q. Lu, J. B. Schenkman and J. F. Rusling, *Journal of the Chemical Society-Faraday Transactions*, 1997, **93**, 1769-1774.
52. V. V. Shumyantseva, T. V. Bulko, Y. O. Rudakov, G. P. Kuznetsova, N. F. Samenkova, A. V. Lisitsa, I. T. Karuzina and A. I. Archakov, *Journal of Inorganic Biochemistry*, 2007, **101**, 859-865.
53. E. V. Suprun, F. Arduini, D. Moscone, G. Palleschi, V. V. Shumyantseva and A. I. Archakov, *Electroanalysis*, 2012, **24**, 1923-1931.
54. A. E. Bard and L. R. Faulkner, *Electrochemical methods: fundamentals and applications*, John Wiley & Sons, New York, 2-nd ed. edn., 2001.
55. C. Leger, S. J. Elliott, K. R. Hoke, L. J. C. Jeuken, A. K. Jones and F. A. Armstrong, *Biochemistry*, 2003, **42**, 8653-8662.
56. E. Laviron, *Journal of Electroanalytical Chemistry*, 1979, **101**, 19-28.
57. UniProtKB, http: //www. uniprot.org.
58. E. Suprun, T. Bulko, A. Lisitsa, O. Gnedenko, A. Ivanov, V. Shumyantseva and A. Archakov, *Biosensors & Bioelectronics*, 2010, **25**, 1694-1698.
59. E. V. Suprun, A. L. Shilovskaya, A. V. Lisitsa, T. V. Bulko, V. V. Shumyantseva and A. I. Archakov, *Electroanalysis*, 2011, **23**, 1051-1057.
60. V. V. Shumiantseva, T. V. Bulko, M. I. Vagin, E. V. Suprun and A. I. Archakov, *Biochemistry (Moscow) Supplement Series B., Biomedical Chemistry*, 2010, **4**, 237-242.
61. E. V. Suprun, A. A. Saveliev, G. A. Evtugyn, A. V. Lisitsa, T. V. Bulko, V. V. Shumyantseva and A. I. Archakov, *Biosensors & Bioelectronics*, 2012, **33**, 158-164.

**TOC graph:**
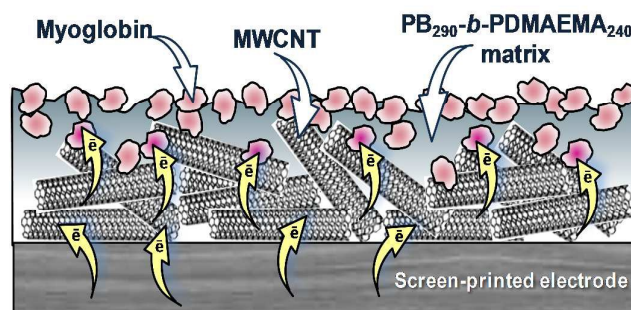


Sequential drop casting of a MWCNTs suspension and a micellar solution of an amphiphilic diblock copolymer onto an electrode results in a favorable nanocomposite for further integration of myoglobin. This facilitates a direct electron transfer from the electrode to the heme protein.